

---

---

# First-in-Human Evaluation of $^{18}\text{F}$ -PF-06445974, a PET Radioligand That Preferentially Labels Phosphodiesterase-4B

Yuichi Wakabayashi<sup>1</sup>, Per Stenkrona<sup>2</sup>, Ryosuke Arakawa<sup>2</sup>, Xuefeng Yan<sup>1</sup>, Maia G. Van Buskirk<sup>1</sup>, Madeline D. Jenkins<sup>1</sup>, Jose A. Montero Santamaria<sup>1</sup>, Kevin P. Maresca<sup>3</sup>, Akihiro Takano<sup>2</sup>, Jehi-San Liow<sup>1</sup>, Thomas A. Chappie<sup>3</sup>, Andrea Varrone<sup>2</sup>, Sangram Nag<sup>2</sup>, Lei Zhang<sup>3</sup>, Zoë A. Hughes<sup>3</sup>, Christopher J. Schmidt<sup>3</sup>, Shawn D. Doran<sup>3</sup>, Andrew Mannes<sup>4</sup>, Paolo Zanotti-Fregonara<sup>1</sup>, Maarten Ooms<sup>1</sup>, Cheryl L. Morse<sup>1</sup>, Sami S. Zoghbi<sup>1</sup>, Christer Halldin<sup>2</sup>, Victor W. Pike<sup>1</sup>, and Robert B. Innis<sup>1</sup>

<sup>1</sup>Molecular Imaging Branch, NIMH-NIH, Bethesda, Maryland; <sup>2</sup>Department of Clinical Neuroscience Psychiatry Section, Karolinska Institutet, Stockholm, Sweden; <sup>3</sup>Worldwide Research, Development, and Medicine, Pfizer Inc., New York, New York; and <sup>4</sup>Anesthesia Department, NIH Clinical Center, Bethesda, Maryland

---

Phosphodiesterase-4 (PDE4), which metabolizes the second messenger cyclic adenosine monophosphate (cAMP), has 4 isozymes: PDE4A, PDE4B, PDE4C, and PDE4D. PDE4B and PDE4D have the highest expression in the brain and may play a role in the pathophysiology and treatment of depression and dementia. This study evaluated the properties of the newly developed PDE4B-selective radioligand  $^{18}\text{F}$ -PF-06445974 in the brains of rodents, monkeys, and humans. **Methods:** Three monkeys and 5 healthy human volunteers underwent PET scans after intravenous injection of  $^{18}\text{F}$ -PF-06445974. Brain uptake was quantified as total distribution volume ( $V_T$ ) using the standard 2-tissue-compartment model and serial concentrations of parent radioligand in arterial plasma. **Results:**  $^{18}\text{F}$ -PF-06445974 readily distributed throughout monkey and human brain and had the highest binding in the thalamus. The value of  $V_T$  was well identified by a 2-tissue-compartment model but increased by 10% during the terminal portions (40 and 60 min) of the monkey and human scans, respectively, consistent with radiometabolite accumulation in the brain. The average human  $V_T$  values for the whole brain were  $9.5 \pm 2.4 \text{ mL} \cdot \text{cm}^{-3}$ . Radiochromatographic analyses in knockout mice showed that 2 efflux transporters—permeability glycoprotein (P-gp) and breast cancer resistance protein (BCRP)—completely cleared the problematic radiometabolite but also partially cleared the parent radioligand from the brain. In vitro studies with the human transporters suggest that the parent radioligand was a partial substrate for BCRP and, to a lesser extent, for P-gp. **Conclusion:**  $^{18}\text{F}$ -PF-06445974 quantified PDE4B in the human brain with reasonable, but not complete, success. The gold standard compartmental method of analyzing brain and plasma data successfully identified the regional densities of PDE4B, which were widespread and highest in the thalamus, as expected. Because the radiometabolite-induced error was only about 10%, the radioligand is, in the opinion of the authors, suitable to extend to clinical studies.

**Key Words:** phosphodiesterase-4B (PDE4B); PET;  $^{18}\text{F}$ -PF-06445974

**J Nucl Med 2022; 63:1919–1924**

DOI: 10.2967/jnumed.122.263838

**P**hosphodiesterase type 4 (PDE4) metabolizes and thereby inactivates the ubiquitous second messenger 3',5'-cyclic adenosine monophosphate (cAMP). PDE4 inhibitors are approved to treat 2 peripheral inflammatory disorders (chronic obstructive pulmonary disease and psoriasis) and are being explored as treatments for several neuropsychiatric disorders (1). PDE4 has 4 isozymes: PDE4A, PDE4B, PDE4C, and PDE4D; of these, the PDE4B and PDE4D isozymes are highly expressed in the brain and may play important roles in pathophysiology and treatment. Interestingly, inhibition of the PDE4D isozyme was found to improve cognition in animals and humans (2), whereas inhibition of the PDE4B isozyme had antidepressantlike effects in animal models (3). Subtype-selective inhibitors not only may be useful in treating distinct disorders but also may avoid the nausea and vomiting associated with nonselective inhibitors. For example, antidepressant trials of the nonselective PDE4 inhibitor rolipram were discontinued because of severe nausea and vomiting.

The search for subtype-selective PDE4 inhibitors has progressed in parallel with the development of comparable PET radioligands that can measure subtype density and evaluate whether the therapeutic candidate crosses the blood–brain barrier and engages the target—that is, receptor occupancy. Subtype-selective PET radioligands have been developed for PDE4B (the subject of this article) and PDE4D. However, the most promising PDE4D radioligand,  $^{11}\text{C}$ -T1650, generated such a significant accumulation of radiometabolites in animal and human brains that it was not recommended for further study (4). Such radiometabolites are problematic because quantitation of the target density is based on the assumption that all radioactivity in the brain is parent radioligand. If radiometabolites are included in brain signal, the density of the target will be overestimated.

$^{18}\text{F}$ -PF-06445974, a new PET radioligand (Supplemental Fig. 1; supplemental materials are available at <http://jnm.snmjournals.org>), was developed to bind preferentially to PDE4B (5). This ligand was selected as a candidate on the basis of its in vitro properties and in vivo performance. In vitro,  $^{18}\text{F}$ -PF-06445974 has high affinity (<1 nM) for PDE4B and moderate-to-high selectivity relative to the other 3 PDE4 subtypes (4.7 nM for PDE4A, 17 nM for PDE4C, and 36 nM for PDE4D). In vivo, PET imaging of  $^{18}\text{F}$ -PF-06445974 in cynomolgus monkeys showed good brain uptake, a high percentage of specific (i.e., blockable) binding, and robust quantitation of enzyme density using arterial input function of

---

Received Jan. 10, 2022; revision accepted Mar. 31, 2022.  
For correspondence or reprints, contact Robert Innis (robert.innis@nih.gov).  
Published online Jun. 30, 2022.  
COPYRIGHT © 2022 by the Society of Nuclear Medicine and Molecular Imaging.

parent radioligand separated from radiometabolite (5). Because of successful imaging in monkeys, the ligand was selected for first-in-human evaluation.

## MATERIALS AND METHODS

This study sought to determine whether  $^{18}\text{F}$ -PF-06445974 could accurately quantify PDE4B in living human brain. Toward this end, PET imaging was performed in healthy human volunteers using the gold standard method of compartmental modeling and serial concentrations of arterial plasma of parent radioligand separated from radiometabolite. Five volunteers were studied: 3 at the National Institutes of Health (NIH) and 2 at the Karolinska Institutet (KI). All participants gave written informed consent, and the study was approved by the institutional review boards of the respective institutions. To address the issue of potential radiometabolite accumulation in the brain, *in vivo* studies in monkeys and *in vivo* and *ex vivo* studies in rodents were also performed after  $^{18}\text{F}$ -PF-06445974 injection and blockade by nonradioactive PF-06445974. A detailed description of the methods and the relevant references (6–11) can be found in the supplemental materials.

## RESULTS

### Brain Imaging

Uptake in the human brain was widespread (peak whole brain SUV, ~2–3) and highest in the thalamus (Figs. 1 and 2), consistent with the distribution of PDE4B (12). Plasma parent concentrations peaked immediately after injection and rapidly decreased along a curve that was well-fitted by a triexponential function (Fig. 2A). Brain activity achieved relatively stable peak values at 15–20 min and washed out slowly thereafter—that is, only 17% washout from 20 to 120 min.

To quantify the density of the target enzyme in brain regions, pharmacokinetic modeling was performed using the serial concentrations of the parent radioligand in arterial plasma as the input to the brain—that is, it was assumed that the brain contains only parent

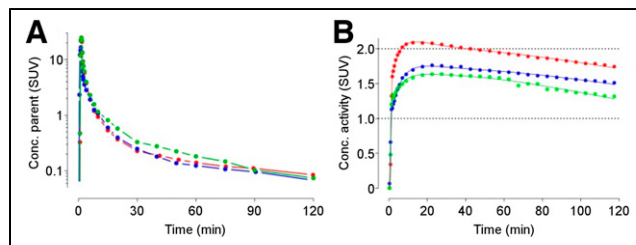


**FIGURE 2.** Concentration of plasma parent radioligand  $^{18}\text{F}$ -PF-0644974 separated from radiometabolite (A) and total radioactivity (B) in whole brain of 3 healthy human participants. The plasma time–activity curve after peak was fit to a triexponential curve. The brain time–activity curve was fit to a 2-tissue-compartment model. Concentrations in plasma and brain are expressed as SUV. Plasma parent is plotted on a log scale, and brain activity is plotted on a linear scale. Conc. = concentration.

radioligand and no radiometabolite. The standard 2-tissue-compartment model provided curves that visually fit the measured PET values in a moderately good to excellent manner (Fig. 2B). Total distribution volume ( $V_T$ ) ( $\text{mL} \cdot \text{cm}^{-3}$ ) ranged from 6.4 in the corpus callosum to 13.3 in the thalamus (Table 1). The variability (SD) of the  $V_T$  measurements was quite large and due in part to differences between the 2 institutions. For example, for the  $V_T$  ( $\text{mL} \cdot \text{cm}^{-3}$ ) of whole brain in the 5 participants reported in Table 1, the NIH values were generally slightly lower (9.9, 9.9, 5.6) than those of the KI (10.2, 12.0). We do not know the cause(s) of these institutional differences but, in such a small population of participants, they could be due to chance. The  $V_T$  in the human brain did not become stable during the 120-min scan. Instead,  $V_T$  values increased by approximately 10% during the last 40 min of the scan (80–120 min; Fig. 3A). This increase was similar in regions with high and low binding (Supplemental Fig. 2).

Brain imaging in 3 monkeys (1 rhesus monkey at the NIH and 2 cynomolgus monkeys at the KI) mirrored that in humans, including the indirect measure of radiometabolite accumulation. That is,

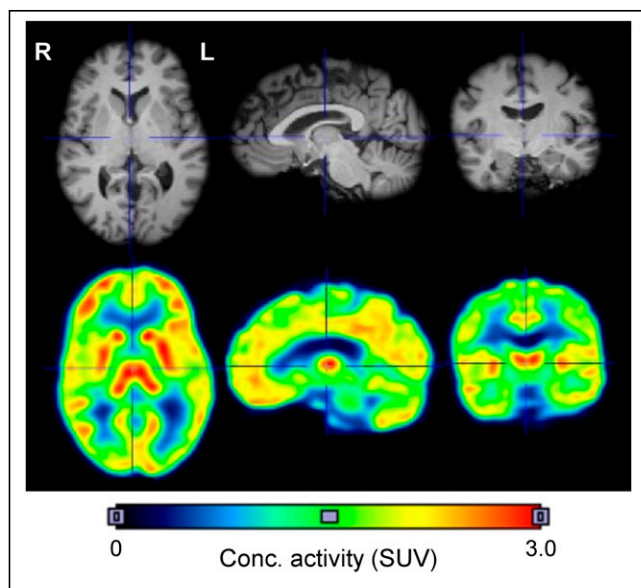


**FIGURE 1.** Distribution of radioactivity in the brain of a healthy volunteer after injection of  $^{18}\text{F}$ -PF-06445974 and the participant’s coregistered MRI scan (top). The PET image displays the mean concentration (conc.) of radioactivity from 0 to 120 min and is expressed as SUV (bottom). The highest uptake was in the thalamus, which is marked with cross hairs.

**TABLE 1**

Total Distribution Volume ( $V_T$ ) in Brain Regions for 5 Human Participants

| Region           | $V_T$ ( $\text{mL} \cdot \text{cm}^{-3}$ ) |     |
|------------------|--|-----|
|                  | Mean                                       | SD  |
| Whole brain      | 9.5  | 2.4 |
| Frontal cortex   | 9.5  | 2.6 |
| Cingulate        | 9.8  | 3.2 |
| Hippocampus      | 9.0  | 2.0 |
| Amygdala         | 11.2                                       | 2.5 |
| Temporal cortex  | 9.8  | 2.0 |
| Parietal cortex  | 9.3  | 2.7 |
| Occipital cortex | 8.9  | 2.2 |
| Striatum         | 12.1                                       | 2.7 |
| Thalamus         | 13.3                                       | 3.4 |
| Globus pallidus  | 12.2                                       | 5.6 |
| Corpus callosum  | 6.4  | 3.8 |
| Insula           | 10.8                                       | 2.7 |
| Cerebellum       | 10.6                                       | 2.2 |

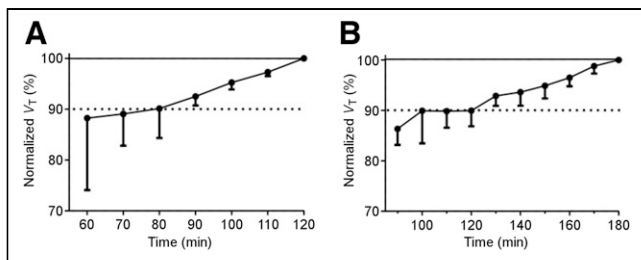


**FIGURE 3.** The apparent value of total distribution volume ( $V_T$ ) from 5 human participants (A) and 3 monkeys (B).  $V_T$  values never achieved stability during the scans.  $V_T$  values increased linearly by 10% during the last 40 min in humans and also by 10% during the last 60 min in monkeys.

$V_T$  increased by about 10% during the last 60 min of the scan (120–180 min; Fig. 3B).

### Assessing Radiometabolite Entry into Brain

The number of radiometabolite peaks in plasma varied among rats, monkeys, and humans, but all radiometabolites were less lipophilic than the parent radioligand, as shown by eluting earlier in the reversed-phase high-performance liquid chromatography (Supplemental Fig. 3). Although less lipophilic, the major radiometabolite peak (marked with an asterisk in Supplemental Fig. 3) eluted close enough to the parent radioligand that it would have been expected to enter the brain.

To directly determine whether this radiometabolite entered the brain, 3 rats were euthanized 180 min after radioligand injection, and radioactivity was extracted from the brain and plasma. Virtually all ( $98\% \pm 2\%$ ) radioactivity in brain coeluted with the parent radioligand, whereas only 32% in plasma was parent radioligand (Fig. 4). Thus, essentially none of the radiometabolite in rat plasma at 180 min was present in the brain.

To explain why rat brain had virtually no radiometabolite, brain uptake was measured in mice with a knockout of both permeability glycoprotein (P-gp) and breast cancer resistance protein (BCRP), the 2 most prevalent efflux transporters at the blood–brain barrier (13). Both the parent radioligand and the chromatographically adjacent radiometabolite were substrates for one or both efflux transporters in mice (Supplemental Fig. 4). At 120 min after  $^{18}\text{F}$ -PF-06445974 injection, the ratio of parent radioligand in brain to that in plasma was 93 in wild-type mice and 188 in knockout mice (Fig. 5); because the concentrations in brain and plasma were in the same unit (SUV), the

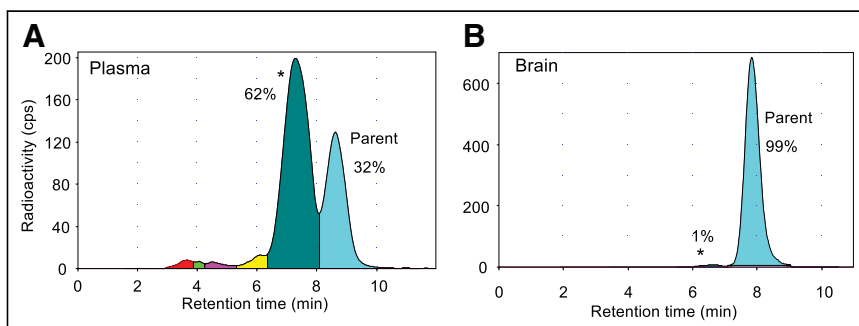


**FIGURE 4.** Radiochromatograms showing the composition of radioactivity extracted at 180 min from plasma (A) and brain (B) of a rat injected with  $^{18}\text{F}$ -PF-06445974. In plasma (A), parent radioligand (blue peak) comprised 32% of total radioactivity, and the adjacent radiometabolite (peak marked with an asterisk) was 62%. At the same time, in the brain (B), parent radioligand comprised 99% of total radioactivity, and the adjacent radiometabolite was only 1%.

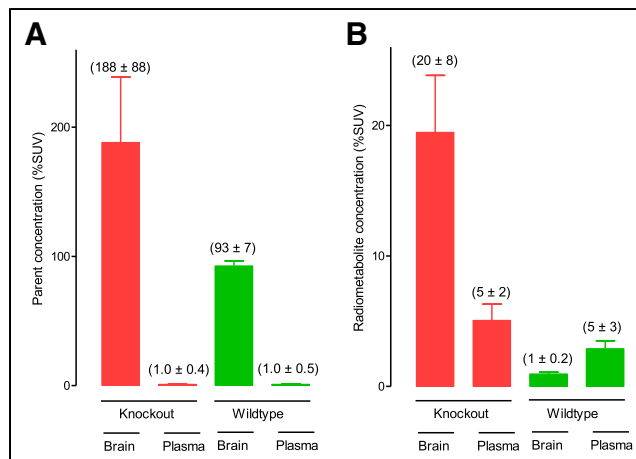


**FIGURE 5.** Concentrations of parent radioligand in brain and plasma of wild-type and efflux transporter knockout mice at 120 min after  $^{18}\text{F}$ -PF-06445974 injection. (A) For the parent radioligand, the ratio of brain-to-plasma concentration was 93 in wild-type and 188 in mice with a knockout of both BCRP and P-gp. Thus, the brain-to-plasma ratio of parent radioligand was 2 times higher in knockout mice than in wild-type mice. (B) For the radiometabolite, the ratio of brain-to-plasma concentration was 0.2 in wild-type and 4.0 in BCRP and P-gp knockout mice. Thus, the brain-to-plasma ratio of parent radioligand was 20 times higher in knockout mice than in wild-type mice. Concentrations are expressed as percent SUV (%SUV).

ratio is unitless. Thus, the brain-to-plasma ratio of parent radioligand was 2 times higher in knockout mice than in wild-type mice. Because these ratios of parent radioligand to brain to plasma were so high, this experiment was repeated in an additional set of 3 animals; similar results were obtained.

In these same mice at 180 min, the ratio of radiometabolite in brain to that in plasma was 0.2 in wild-type and 4.0 in knockout mice (i.e., a 20-fold difference), indicating that knockout of these 2 transporters had about a 10-fold greater effect (20 vs. 2) on the radiometabolite than on the parent radioligand. This differential effect on the radiometabolite versus the parent radioligand was also seen in the percentage composition of radioactivity in the brain at 120 min. Specifically, the percentage of radiometabolite in the brain was about 5-fold higher in knockout (8.8%) than in wild-type (1.8%) mice (Supplemental Table 1).

Because substrate specificity varies between species, avidity was measured *in vitro* using cloned human transporters and compared with known substrates: digoxin for P-gp and prazosin for BCRP.

For BCRP, prazosin had an efflux ratio of 9.2 whereas PF-06445974 had a ratio of 5.9 (Supplemental Table 2), suggesting that PF-06445974 was a mild/moderate substrate for BCRP. In contrast, PF-06445974 was a far less avid substrate for P-gp; specifically, digoxin had an efflux ratio of 38.1, and PF-06445974 had a ratio of only 2.5—that is, less than 1/15th that for digoxin.

Like all metabolites, radiometabolites are often pharmacologically inactive by virtue of low affinity for the target protein. Thus, any displaceable binding typically reflects parent radioligand rather than radiometabolite. Non-radioactive PF-06445974 (0.1 mg/kg intravenously injected 10 min before the radioligand) blocked almost all radioactivity in rat and

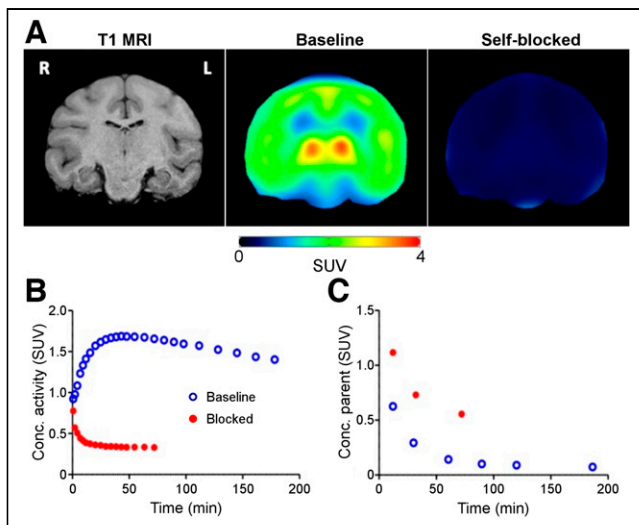


**FIGURE 6.** (A) PET and coregistered MRI of brain in a rhesus monkey. The animal was scanned at baseline and after blockade by PF-06445974 (0.1 mg/kg intravenously injected 10 min before radioligand). Because of prolonged tachycardia (heart rate up to 190 bpm), the blocked scan was terminated after 75 min. The PET images show mean concentration of radioactivity SUV from 0 to 70 min. (B) Radioactivity in whole brain after injection of  $^{18}\text{F}$ -PF-06445974. (C) Concentration in arterial plasma of plasma parent radioligand  $^{18}\text{F}$ -PF-06445974 separated from radiometabolite. Because there were so few plasma samples, compartmental modeling could not generate a reliable measure of enzyme density (total distribution volume,  $V_T$ ). Measured as average concentration of radioactivity from 10 to 60 min (SUV<sub>10-60</sub>), nonradioactive PF-06445974 blocked 92% of radioligand uptake into brain. Conc. = concentration.

monkey brain for the entire duration of the scan (Fig. 6; Supplemental Fig. 5). For the rhesus monkey, nonradioactive PF-06445974 decreased SUV<sub>10-60</sub> by 92% in the whole brain (Fig. 6). In rats, nonradioactive PF-06445974 decreased SUV<sub>10-180</sub> by 94% in the whole brain (Supplemental Fig. 5).

In summary, plasma from rats, monkeys, and humans showed a range of radiometabolites, all with lower—though sometimes only slightly lower—lipophilicities than that of  $^{18}\text{F}$ -PF-06445974. None of these radiometabolites was present in rat brain 180 min after injection. Studies in knockout mice showed that the radiometabolite (the peaks marked with an asterisk in Fig. 4 and Supplemental Fig. 3) adjacent to the radioligand was avidly cleared from the brain by P-gp or BCRP (Supplemental Fig. 4). The monkey studies showed that 92% of brain radioactivity was blocked by nonradioactive ligand, suggesting that most of the radioactivity in monkey brain, like that in rats and mice, represented parent radioligand. Thus, by analogy to rats and monkeys, it is likely that no more than a small amount of radiometabolite ( $\leq 10\%$  of total radioactivity) accumulates in the human brain. However, of particular importance to the quantitation of enzyme density, the *in vitro* studies showed that the parent radioligand is a moderate substrate for human BCRP.

#### Dosimetry Calculations in Human and Nonhuman Primates

Whole-body imaging in 2 humans and 1 monkey was notable for early distribution in the blood pool, accumulation in the target organs (i.e., brain and lung), and excretion via the urinary tract (Supplemental Fig. 6). For the human volunteers, the 4 organs with the highest exposure ( $\mu\text{Sv}/\text{MBq}$ ) were gallbladder ( $110 \pm 75$ ), upper large intestine ( $75 \pm 66$ ), urinary bladder ( $55 \pm 5.9$ ), and liver ( $44 \pm 8.1$ ). The doses in the 2 humans were 19.6 and 19.3  $\mu\text{Sv}/\text{MBq}$ ,

respectively, which were similar to those extrapolated from monkeys (16.5  $\mu\text{Sv}/\text{MBq}$ ) (Supplemental Table 3).

#### DISCUSSION

This study sought to determine whether  $^{18}\text{F}$ -PF-06445974 could accurately quantify PDE4B in human brain. Our results suggest that this radioligand quantified PDE4B reasonably well, with the exception that radiometabolite likely accumulated in the brain and that the radioligand itself may be a substrate for efflux transport from the brain. Brain uptake was moderately high (peak whole-brain SUV was 1.5), and its distribution was appropriate for the target. The PET measurements of enzyme binding ( $V_T$ ) from the human brain were reasonably well fit to a 2-tissue-compartment model that assumed input of only the parent radioligand from arterial plasma. The  $V_T$  value increased by approximately 10% over the last 60 min of the 120-min scan (Fig. 3), which may have been caused by radiometabolite accumulation in the brain.

To directly measure radiometabolite, all radioactivity was extracted from the plasma and brain of rats at 180 min and the components were separated using radio-high-performance liquid chromatography. Surprisingly, rat brain contained essentially no radiometabolite, although the plasma had several radiometabolites, one of which eluted only slightly before the parent radioligand. Knockout of 2 efflux transporters (P-gp and BCRP) in mice showed that the radiometabolite was avidly cleared from the brain and that the parent radioligand was also a substrate, but of lower avidity. Thus, either or both efflux transporters had the positive effect of “cleaning up” the brain signal by removing radiometabolite, but also the negative effect of removing some of the parent radioligand. *In vitro* studies using cloned human efflux transporters showed that PF-06445974 was a moderate substrate for BCRP and, to a lesser extent, for P-gp. Although these efflux transporters completely cleared radiometabolite from rodent brain, they likely did so only partially in humans, leading to the accumulation of the adjacent radiometabolite in human brain, as shown by increasing values of enzyme density with increasing length of scanning.

Compartmental modeling seeks to measure the specific binding ( $V_S$ ) of the radioligand for the target and is proportional to receptor density ( $B_{\text{max}}$ ) times the radioligand’s affinity ( $1/K_D$ ). Because the measurements of PET radioactivity in brain and of parent radioligand in plasma have noise, a substantial number of such measurements are required to converge on a value of specific binding, often 15–60 min for many brain radioligands. If the density of the target and the affinity of the radioligand remain constant during the scan, the converged/well-identified  $V_S$  value should not change with increasing scan duration, which will be reflected by the brain and plasma time-activity curves decreasing at the same rate. In contrast, in this study, values of total uptake ( $V_T = V_S + V_{\text{ND}}$ ) appeared to increase with increasing scan duration.

The 2 most common causes of unstable  $V_T$  values are slow kinetics of radioligand binding or the accumulation of radiometabolites in the brain. The first possible cause, slow kinetics, refers to how long the radioligand requires to reach equilibrium, which in this case usually refers to the time of peak radioactivity in brain; note that the term “peak equilibrium” refers to tissue-to-plasma ratio at the exact time of peak uptake in the brain, which varies among regions. This peak equilibrium is distinct from “transient equilibrium” (14), which refers to the tissue-to-plasma ratio after the time of peak uptake and which is typically greater than the true  $V_T$ . As a rule, the brain must be imaged before, at, and for some time after peak uptake to quantify the rates of binding and unbinding to the receptor, which themselves

are components of  $V_T$ . Here, the time to peak was about 30 min in monkeys and 20 min in humans, and our scans extended well beyond the peak (for a total of 180 min in monkeys and 120 min in humans), suggesting that slow kinetics of radioligand binding are unlikely to have caused the  $V_T$  values that increased with scan duration. Instead, radiometabolite probably accumulated in the human brain. The likely candidate is the peak marked with an asterisk in Supplemental Figure 3, which has a lipophilicity only slightly lower than that of the parent radioligand.

It should be noted that being a substrate for efflux transport is unlikely to increase  $V_T$  values over time, as it is predicted to have the opposite result. That is, the effect of efflux transport is to decrease radioactivity in the brain and, therefore, to decrease the apparent  $V_T$ . Nevertheless, the time course of efflux transport of parent ligand and radiometabolite might change in some unexpected way to contribute to increasing apparent values of  $V_T$ .

Taken together, the results suggests that the 2 pharmacologic limitations of  $^{18}\text{F}$ -PF-06445974 for quantifying PDE4B in human brain are the accumulation of a radiometabolite in the brain and partial removal of the parent radioligand by the efflux transporter BCRP. Both pharmacologic limitations will increase the variability of the measurements between individuals to the extent that individuals differ in metabolism and BCRP function. The severity of these combined limitations in humans is unknown but, in the opinion of the authors, would not preclude using this radioligand in clinical studies. An increase in  $V_T$  of  $< 5\%$  during the last hour is considered excellent, and our rate of 10% in the last 60 min (Fig. 3) is generally considered acceptable. Notably, this 10% variability mirrors what might maximally occur based on blockade studies in monkeys (Fig. 6). That is, nonradioactive PF-06445974 blocked 92% of total uptake in monkey brain, suggesting that 92% of radioactivity in brain was parent radioligand; metabolites usually, but not always, have lower affinity for the target than the parent drug.

Although these 2 limitations will increase the necessary sample size for a clinical study, we will proceed with use of this radioligand to study clinical disorders such as major depressive disorder (MDD) for 2 reasons. First, as described earlier, the error/variability of these limitations may be only about 10%. Second, PET imaging of PDE4 provides the unique ability to measure the activated (i.e., phosphorylated) form of PDE4, which is not possible in post-mortem samples (Fig. 7). Prior studies in this laboratory with  $^{11}\text{C}$ -(*R*)-rolipram, which binds to all 4 PDE4 subtypes, provide in vivo support for the notion that cAMP increases radioligand binding via phosphorylation of PDE4 by protein kinase A (15). This phosphorylation increases enzyme activity as well as the affinity of radioligand binding by about 10-fold (16). Because PDE4 is rapidly dephosphorylated after death (17), PET is uniquely capable of measuring the active form of PDE4 in living participants.

Evidence from the 1980s and 1990s suggested that rolipram might be used to treat MDD, and animal models of depression suggested that PDE4B inhibitors might have antidepressant efficacy in humans (3). In this context, a PET radioligand for PDE4B could facilitate therapeutic drug development. For instance, we predict that the current study using a PDE4B-selective radioligand will replicate results previously obtained with the nonselective radioligand  $^{11}\text{C}$ -(*R*)-rolipram (18)—namely, that PDE4B binding will be decreased in unmedicated individuals experiencing a major depressive episode but still have significant overlap with that in healthy volunteers. If so, this PDE4B radioligand could be used to identify a subgroup of MDD patients who would most benefit from PDE4B inhibition, given that low PDE4 binding implies low cAMP signaling because

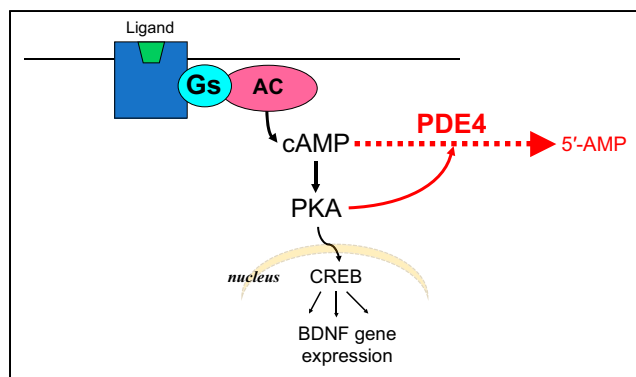


**FIGURE 7.** Schema of the cAMP cascade (black arrows) and negative feedback via protein kinase A (PKA) (red arrows). Several neurotransmitters act via receptors coupled to G proteins (Gs) to stimulate adenylyl cyclase (AC), which produces cAMP, activates PKA, and then phosphorylates cAMP response element-binding protein (CREB), which moves to the nucleus and increases expression of brain-derived neurotrophic factor (BDNF) and other genes. Negative feedback is provided by PKA, which phosphorylates and activates PDE4, which metabolizes cAMP, thereby terminating the cAMP signal.

of the negative feedback mechanism mediated by protein kinase A. The cAMP theory of the mechanism of antidepressant treatments would further suggest that increasing cAMP signaling produces antidepressant effects. Thus, those patients with low PDE4B binding might be most likely to benefit from treatment with a PDE4B inhibitor. Furthermore, numerous animal studies have shown that antidepressants of all chemical classes must be administered for several weeks in order to upregulate the cAMP cascade (19), which mirrors the therapeutic time course in humans. Because inhibiting PDE4B would immediately increase cAMP signaling, these antidepressant effects, if they exist, would occur quickly, meaning that PDE4B inhibitors may represent a new class of rapid-acting antidepressants.

In short, a PET radioligand for PDE4B may be useful in 2 ways. First, if a PDE4B inhibitor is developed as an antidepressant medication, the PET radioligand can be used to identify the appropriate dose and dosing interval of the therapeutic candidate. Indeed, PET radioligands have often been used to measure receptor occupancy and guide initial doses in therapeutic trials. Second, a PDE4B radioligand might identify a subgroup of patients most likely to respond to a PDE4B inhibitor. This selection of patients likely to respond has been referred to as patient stratification, patient enrichment, personalized medicine, and, most recently, precision medicine. Expressed in other terms, low PDE4B binding may be a biomarker to predict response to a PDE4B inhibitor.

## CONCLUSION

$^{18}\text{F}$ -PF-06445974 was able to quantify PDE4B in human brain with reasonable, but not complete, success. The gold standard compartmental method of analyzing brain and plasma data successfully identified the regional densities of PDE4B, which were widespread and highest in the thalamus, as expected. Although a radiometabolite may contaminate the signal in human brain, the amount is likely small enough ( $\sim 10\%$ ) that the authors plan to use this radioligand in clinical studies.

## DISCLOSURE

This study was funded by the Intramural Research Program of the National Institute of Mental Health (projects ZIAMH002852

and ZIAMH002793; animal protocol: MIB-02) and by a research contract from Pfizer to the Karolinska Institutet. Per Stenkrona, Ryosuke Arakawa, Akihiro Takano, Andrea Varrone, Sangram Nag, and Christer Halldin were supported by a contract with Pfizer. Kevin P. Maresca, Thomas A. Chappie, Lei Zhang, Zoë A. Hughes, Christopher J. Schmidt, and Shawn D. Doran are full-time employees of Pfizer. No other potential conflict of interest relevant to this article was reported.

## ACKNOWLEDGMENTS

We are grateful to the staff of Molecular Imaging Branch for participant recruitment; to the NIH's PET Department (Chief, Peter Herscovitch, MD) for performing the PET scans; to Ioline Henter for invaluable editorial assistance; and to Cerevel Therapeutics for obtaining the in vitro potencies of PF-06445974 at human P-gp and BCRP transporters.

## KEY POINTS

**QUESTION:** Can  $^{18}\text{F}$ -PF-06445974 accurately quantify PDE4B in living human brain?

**PERTINENT FINDINGS:**  $^{18}\text{F}$ -PF-06445974 can accurately quantify PDE4B, except for the likely presence of a small amount (probably ~10%) of radiometabolite in the brain and the removal of the radioligand from the brain via an efflux transporter.

**IMPLICATIONS FOR PATIENT CARE:** These findings have no direct implications for clinical care. However, a radioligand selective for PDE4B could measure this target in clinical disorders and facilitate the development of PDE4B-selective inhibitors as novel therapeutics.

## REFERENCES

- Menniti FS, Faraci WS, Schmidt CJ. Phosphodiesterases in the CNS: targets for drug development. *Nat Rev Drug Discov*. 2006;5:660–670.
- Berry-Kravis EM, Harnett MD, Reines SA, et al. Inhibition of phosphodiesterase-4D in adults with fragile X syndrome: a randomized, placebo-controlled, phase 2 clinical trial. *Nat Med*. 2021;27:862–870.
- Zhang C, Xu Y, Zhang H-T, Gurney ME, O'Donnell JM. Comparison of the pharmacological profiles of selective PDE4B and PDE4D inhibitors in the central nervous system. *Sci Rep*. 2017;7:40115.
- Wakabayashi Y, Telu S, Dick RM, et al. Discovery, radiolabeling, and evaluation of subtype-selective inhibitors for positron emission tomography imaging of brain phosphodiesterase-4D. *ACS Chem Neurosci*. 2020;11:1311–1323.
- Zhang L, Chen L, Beck EM, et al. The discovery of a novel phosphodiesterase (PDE) 4B-preferring radioligand for positron emission tomography (PET) imaging. *J Med Chem*. 2017;60:8538–8551.
- Hammers A, Allom R, Koeppe MJ, et al. Three-dimensional maximum probability atlas of the human brain, with particular reference to the temporal lobe. *Hum Brain Mapp*. 2003;19:224–247.
- Innis RB, Cunningham VJ, Delforge J, et al. Consensus nomenclature for in vivo imaging of reversibly binding radioligands. *J Cereb Blood Flow Metab*. 2007;27:1533–1539.
- National Research Council. *Guide for the Care and Use of Laboratory Animals*. 8th ed. Washington, DC: National Academies Press; 2011.
- Sprague DR, Fujita M, Ryu YH, Liow JS, Pike VW, Innis RB. Whole-body biodistribution and radiation dosimetry in monkeys and humans of the phosphodiesterase 4 radioligand [ $^{11}\text{C}$ ](R)-rolipram: comparison of two-dimensional planar, bisected and quadrisectioned image analyses. *Nucl Med Biol*. 2008;35:493–500.
- Terry G, Liow JS, Chemet E, et al. Positron emission tomography imaging using an inverse agonist radioligand to assess cannabinoid CB1 receptors in rodents. *Neuroimage*. 2008;41:690–698.
- Zoghbi SS, Shetty HU, Ichise M, et al. PET imaging of the dopamine transporter with  $^{18}\text{F}$ -FECNT: a polar radiometabolite confounds brain radioligand measurements. *J Nucl Med*. 2006;47:520–527.
- Richter W, Menniti FS, Zhang H-T, Conti M. PDE4 as a target for cognition enhancement. *Expert Opin Ther Targets*. 2013;17:1011–1027.
- Löscher W, Potschka H. Blood-brain barrier active efflux transporters: ATP-binding cassette gene family. *NeuroRx*. 2005;2:86–98.
- Carson RE. PET physiological measurements using constant infusion. *Nucl Med Biol*. 2000;27:657–660.
- Itoh T, Abe K, Hong J, et al. Effects of cAMP dependent protein kinase activator and inhibitor on in vivo PET rolipram binding to phosphodiesterase 4 in conscious rats. *Synapse*. 2010;64:172–176.
- Hoffmann R, Wilkinson IR, McCallum JF, Engels P, Houslay MD. cAMP-specific phosphodiesterase HSPDE4D3 mutants which mimic activation and changes in rolipram inhibition triggered by protein kinase A phosphorylation of Ser-54: generation of a molecular model. *Biochem J*. 1998;333:139–149.
- Itoh T, Abe K, Zoghbi SS, et al. PET measurement of the in vivo affinity of  $^{11}\text{C}$ -(R)-rolipram and the density of its target, phosphodiesterase-4, in brain of conscious and anesthetized rats. *J Nucl Med*. 2009;50:749–756.
- Fujita M, Richards EM, Niciu MJ, et al. cAMP signaling in brain is decreased in unmedicated depressed patients and increased by treatment with a selective serotonin reuptake inhibitor. *Mol Psychiatry*. 2017;22:754–759.
- Duman RS. Synaptic plasticity and mood disorders. *Mol Psychiatry*. 2002;7(suppl 1):S29–S34.